Characteristics of a Si dual-band detector responding in both near- and very-long-wavelength-infrared regions

G. Ariyawansa, M. B. M. Rinzan, S. G. Matsik, G. Hastings, and A. G. U. Perera[a)]
Department of Physics and Astronomy, Georgia State University, Atlanta, Georgia 30303

H. C. Liu, M. Buchanan, and G. I. Sproule
Institute for Microstructural Sciences, National Research Council, Ottawa K1A OR6, Canada

V. I. Gavrilenko
Institute for Physics of Microstructures, 603950 Nizhny Novgorod, Russia

V. P. Kuznetsov
Physical-Technical Research Institute, Nizhny Novgorod State University, Gagarin Avn. 23, 603950 Nizhny Novgorod, Russia

(Received 10 April 2006; accepted 6 July 2006; published online 9 August 2006)

A *p*-type Si homojunction detector responding in both near- and very-long-wavelength-infrared (NIR and VLWIR) ranges is demonstrated. The detector consists of a p^{++}-Si top contact layer, a p^{+}-Si emitter, an undoped Si barrier, and a p^{++}-Si bottom contact layer grown on a Si substrate. Interband and intraband transitions lead to NIR and VLWIR responses, respectively. The responsivity, quantum efficiency, and detectivity at −1 V bias and 4.6 K are ~0.024 A/W, 3.7%, and $\sim 1.7\times 10^{9}$ cm $\mathrm{Hz}^{1/2}$/W at 0.8 μm, while they are 1.8 A/W, 8.8%, and $\sim 1.2\times 10^{11}$ cm $\mathrm{Hz}^{1/2}$/W at 25 μm, respectively. The background limited infrared performance temperature at ±0.9 V bias is 25 K. © *2006 American Institute of Physics*.
[DOI: 10.1063/1.2336202]

Interest in developing multiband detectors[1–5] has increased recently. This is partly due to the increased accuracy in using multiple wavelength bands. For example, in mine detection[6] false positives can be reduced and a missile can be clearly distinguished from its plume. Measuring multiple wavelength bands typically requires multiple detectors with separate cooling assemblies and readout circuits. The difficulties of assembling several detectors and the increased cost can be overcome by using a single detector responding in multiple bands. Recently, GaAs dual-band detectors responding in both the near-/midinfrared (NIR/MIR)[3] and NIR/far-infrared regions[7] have been reported. Here, a *p*-type Si homojunction interfacial workfunction internal photoemission[8] (HIWIP) detector sensitive to NIR and very-long-wavelength infrared (VLWIR) radiation is discussed. In comparison with the GaAs dual-band detector reported previously,[7] this detector has an extended NIR response (up to 1 μm) and a continuous IR response from 5 to 35 μm with a peak at 25 μm. Commercially available Si detectors with a response in the range of 5–30 μm are operated at 4.2 K and have a responsivity of 2 A/W. Si blocked impurity band[9] detectors have a responsivity of 32 A/W at 7 K and previously demonstrated Si HIWIP detectors[10] have shown a responsivity of 12.3 A/W at 27.5 μm with a detectivity of 6.6×10^{10} cm $\mathrm{Hz}^{1/2}$/W at 4.2 K. As a VLWIR detector, this device can be operated at 4.6 K with a responsivity of 1.8 A/W and a detectivity of $\sim 1.2\times 10^{11}$ cm $\mathrm{Hz}^{1/2}$/W at 25 μm under −1 V bias. It also operates up to 30 K with a background limited infrared performance (BLIP) temperature of 25 K at ±0.9 V bias. Although the device is not optimized for either NIR or VLWIR operations, both the NIR and the VLWIR responses together could have a commercial appeal. In astronomy, where infrared technology plays a dominant role in observing celestial objects, the NIR response of the detector can be used to observe cooler red objects and VLWIR can detect cold objects such as comets, planets, etc.

The Si based HIWIP detector was grown by metal-organic chemical-vapor deposition on Si substrate and consists of a *p*-doped Si bottom contact, an undoped Si barrier, a *p*-doped Si emitter layer, and a *p*-doped Si top contact layer, as shown in Fig. 1(a). Boron was used as the *p*-type dopant. The devices were processed and a 400×400 μm^2 device was used for characterization. As shown in Fig. 1(b), the dual-band detection is based on interband transitions in the undoped barrier (NIR), and intraband transition within the emitter (VLWIR). Incident NIR photons are absorbed by the

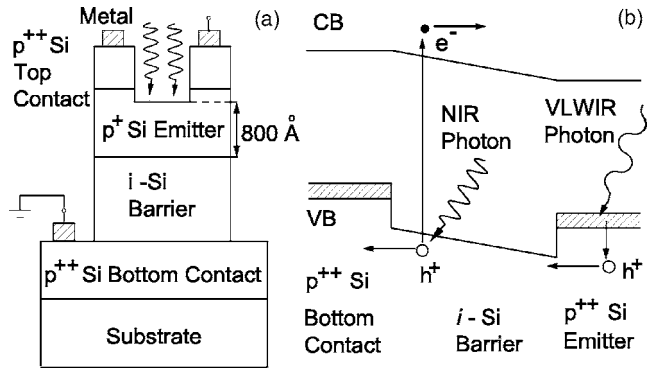

FIG. 1. (a) Schematic diagram of Si HIWIP structure. The doping concentration of the Si emitter is 2.5×10^{18} cm^{-3}, while the contacts are doped to 1.5×10^{19} cm^{-3}. The Si barrier is not intentionally doped. The thicknesses of the top contact, emitter, barrier, and bottom contact layers are 0.1, 0.2, 1, and 1 μm, respectively. (b) Band diagram showing the conduction and valence band profiles of the structure.

[a)]Electronic mail: uperera@gsu.edu

Si barrier layer, and an electron-hole pair is generated. Excited carriers are then collected by the applied electric field and both electrons and holes contribute to the photocurrent. The wavelength threshold is determined by the band gap of the barrier material. The detection mechanism leading to VLWIR detection involves free carrier absorption in the emitter, followed by the internal photoemission of photoexcited carriers, and then the collection of carriers by the applied electric field at the contacts. When the emitter is doped above the Mott transition level, an impurity band is formed and the Fermi level goes below the valence band edge (for p type), making a metallic emitter layer. However, the Fermi level in the emitter still can be above the valence band edge of the barrier due to the band gap narrowing in the emitter from the high doping. The offset between the Fermi level in the emitter layer and the valence band edge of the barrier layer forms the interfacial workfunction (Δ). If the shift of the valence band edge of the emitter with respect to that of the barrier due to band gap narrowing is ΔE_V, and the Fermi level with respect to the valence band edge of the emitter is E_F, then $\Delta=\Delta E_V-E_F$. A detailed explanation is given in Ref. 8. The threshold wavelength λ_t (in μm) is calculated by $1240/\Delta$, where Δ is in meV. Although the Si barrier is not intentionally doped, a slight doping is expected due to dopant migration from the emitter. These hydrogenic impurities give rise to a series of transitions leading to photoresponse peaks.[11]

The spectral response of the detector was obtained for normal incidence radiation using a Perkin Elmer System 2000 Fourier transform infrared spectrometer. The calibration of spectra was performed using an InSb detector in NIR region, and a Si composite bolometer (from 1 μm and above).

The NIR response at −1 V bias shows a threshold at ~1.05 μm, which is in accordance with ~1.17 eV bandgap of Si at 4.6 K, as shown in Fig. 2(a). The two arrows in the figure mark the position of the E_1^{TO} and E_2^{TO} absorption bands that are due to TO-phonon assisted exciton transitions at the band edge.[12] E_1^{TO} is observed at 1.21 eV and the separation between E_1^{TO} and E_2^{TO} is less than 2 meV. Hence E_2^{TO} cannot be observed clearly in the photoresponse curve. A NIR responsivity of 0.024 A/W is obtained at 0.8 μm with a detectivity of $\sim 1.7\times 10^9$ cm Hz$^{1/2}$/W at 0.8 μm under −1 V bias at 4.6 K.

As shown in Fig. 2(b), the VLWIR response arising from intraband transitions at 4.6 K is in the range of 5–35 μm. The threshold wavelength observed at −0.5 V bias is 32 μm, and the corresponding value of $\Delta=38.7$ meV is in good agreement with the theoretical model.[13] Arrhenious calculations based on the dark current also confirm this value of Δ. The threshold wavelength increases with the applied bias, as shown in Fig. 2(b). This is a result of decreasing Δ with increasing bias.[8] The photoresponse shows a strong bias dependence mainly due to field-assisted tunneling of photoexcited carriers. At 25 μm responsivity values at −0.5, −1, and −1.5 V biases are 0.90, 1.78, and 31.0 A/W, respectively. When the bias is increased further, a rapid improvement of the photoresponse can be observed, and Fig. 3(a) shows a responsivity of 157 A/W at 25 μm at −2 V bias, which translates to an efficiency-gain product of 7.8. Highly sensitive NIR detectors with high internal gain have been observed previously.[14,15] Applying a high electric field across the structure enhances the process of impact ionization within the barrier, introducing a gain into the photocurrent.[16]

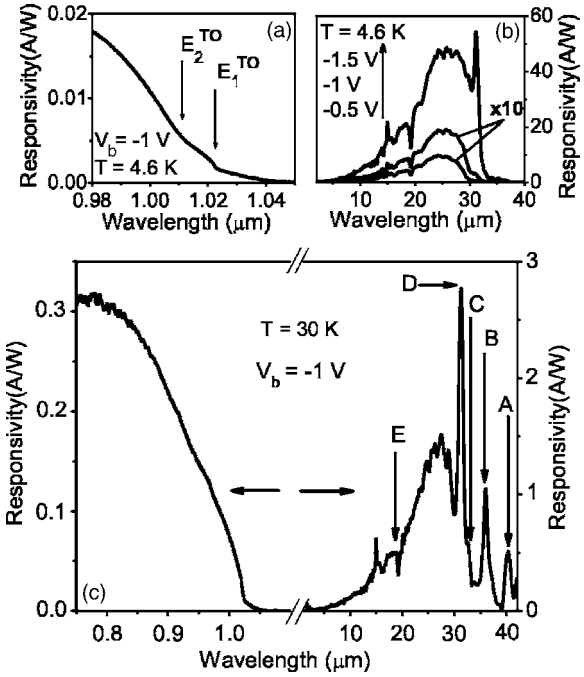

FIG. 2. (a) NIR response of the detector measured at 4.6 K. The two arrows mark the position of two TO-phonon assisted absorption bands. (b) VLWIR response under different bias values at 4.6 K. The curves at −1 and −0.5 V biases have been multiplied by 10. (c) Spectral response of the detector in both the NIR and VLWIR regions, measured at 30 K under −1 V bias. The arrows indicate the positions of impurity transitions of boron in Si (A–D), and the absorption due to the optical phonon in Si (E).

This type of gain mechanism is possible if the barrier contains impurity atoms. The observation of impurity transition peaks to be discussed later is evidence for the existence of impurities in the barrier. Despite the high responsivity obtained at high bias voltages, the optimum detectivity observed is $\sim 1.5\times 10^{11}$ cm Hz$^{1/2}$/W at −1 V bias. This is due to an increase of the noise current with bias. Moreover, Fig. 3(b) shows the variation of the detectivity with temperature at 25 μm under −1 V bias. This behavior of the detectivity with temperature is typical for most of infrared devices since the noise current increases with temperature.

The dual-band response has been obtained up to 30 K, as shown in Fig. 2(c). At −1 V bias and 30 K, the responsivity, quantum efficiency, and detectivity at 0.8 μm are ~0.30 A/W, 46%, and $\sim 6.7\times 10^8$ cm Hz$^{1/2}$/W, while at

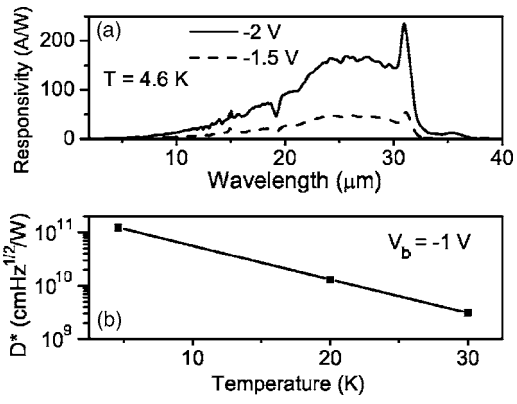

FIG. 3. (a) Responsivity of the detector at 4.6 K under −1.5 and −2 V biases. The observed responsivity of 157 A/W at 25 μm at −2 V indicates a value of 7.8 for the product of quantum efficiency and gain. (b) Detectivity at 25 μm at different temperatures under −1 V bias.

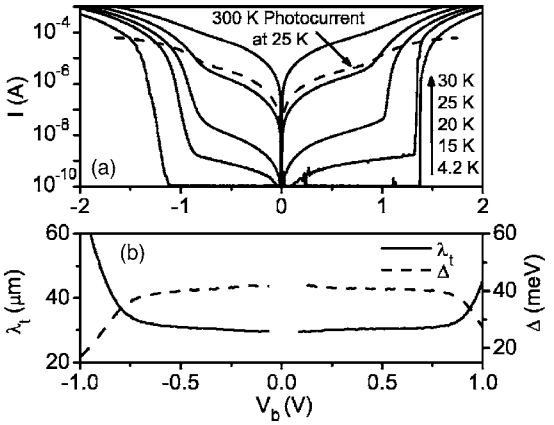

FIG. 4. (a) Dark *IV* characteristics of the detector at different temperatures. The 300 K background photocurrent curve at 25 K is also shown. (b) Calculated activation energy (Δ), and corresponding threshold wavelength (λ_t) with bias, based on the Arrhenius model.

25 μm they are 1.4 A/W, 7%, and $\sim 3.1\times 10^9$ cm $\mathrm{Hz}^{1/2}$/W, respectively. The quantum efficiency can be improved by using a multiperiod design and incorporating a resonant cavity[17] into the structure. The sharp peaks (labeled as A–D) superimposed on the free carrier response become dominant at 30 K. These peaks can be well fitted with the impurity transitions of boron in Si. The intensity of the transition increases with temperature[18] as the efficiency of the photothermal mechanism leading to the excitations increases with temperature. The enhanced response at 30 K and the vanishing of peak A (30.7 meV) at 4.6 K confirm that the relative intensity of the impurity peaks increases with temperature. Merlet *et al.*[11] compared the positions of the peaks reported by several other researchers. In Fig. 2(c), peaks A, B, C, and D observed at 30.7, 34.4, 38.3, and 39.6 meV have been previously reported at 30.37, 34.50, 38.38, and 39.63 meV, respectively, by Merlet *et al.* The deviation of the energy values falls within the spectral resolution. A theoretical calculation of acceptor states of Si along with experimental results have been presented by Onton *et al.*[19] Furthermore, the small absorption dip around 19 μm is due to the optical phonon of Si reported at 63 meV (19.6 μm).

The dark current-voltage (*IV*) characteristics at different temperatures, and the 300 K background photocurrent measured at 25 K are shown in Fig. 4(a). The current increases drastically due to hopping conduction[10] beyond a bias of ±1 V (an electric field of 10 kV/cm). Based on the dark and the photocurrent measurements, performed using a closed cycle refrigerator with a cold shield at 70 K and under 60° field of view, the BLIP temperature at ±0.9 V is determined as 25 K. The activation energy (Δ) was calculated by using the Arrhenius model, and the variation of the calculated Δ and the corresponding λ_t with bias is shown in Fig. 4(b). The calculated λ_t is in good agreement with the observed threshold in the bias range from −0.75 to 0.75 V. Beyond this region, the dark current from tunneling dominates the thermal current, as seen in *IV* curves, and the Arrhenius model diverges, resulting in invalid values for Δ.

In summary, a Si HIWIP dual-band detector responding in both NIR and VLWIR regions was reported. The NIR response can be explained in terms of interband transition in the undoped Si barrier layer in the structure. The NIR wavelength threshold corresponds to the band gap of Si. The VLWIR response arises due to free carrier absorption and intraband transitions within the structure. In addition, the impurity transitions of boron in Si were confirmed. Good performance of the detector demonstrates potential for applications, especially where detection in both the NIR and MIR/VLWIR regions is required.

This work was supported in part by the NSF under Grant Nos. ECS-0553051 and DBI: 0352324. The authors thank P. Chow-Chong and R. Dudek for sample preparation.

[1] H. C. Liu, C. Y. Song, A. Shen, M. Gao, Z. R. Wasilewski, and M. Buchanan, Appl. Phys. Lett. **77**, 2437 (2000).
[2] S. Krishna, G. von Winckel, S. Raghavan, A. Stintz, G. Ariyawansa, S. G. Matsik, and A. G. U. Perera, Appl. Phys. Lett. **83**, 2745 (2003).
[3] M. P. Touse, G. Karunasiri, K. R. Lantz, H. Li, and T. Mei, Appl. Phys. Lett. **86**, 093501 (2005).
[4] J. Li, K. K. Choi, and D. C. Tsui, Appl. Phys. Lett. **86**, 211114 (2005).
[5] S. Chakrabarti, X. H. Su, P. Bhattacharya, G. Ariyawansa, and A. G. U. Perera, IEEE Photonics Technol. Lett. **17**, 178 (2005).
[6] Arnold Goldberg, Parvez N. Uppal, and Michael Winn, Infrared Phys. Technol. **44**, 427 (2003).
[7] G. Ariyawansa, M. B. M. Rinzan, D. G. Esaev, S. G. Matsik, A. G. U. Perera, H. C. Liu, B. N. Zvonkov, and V. I. Gavrilenko, Appl. Phys. Lett. **86**, 143510 (2005).
[8] A. G. U. Perera, H. X. Yuan, and M. H. Francombe, J. Appl. Phys. **77**, 915 (1995).
[9] James E. Huffman, A. G. Crouse, B. L. Halleck, T. V. Downes, and Terry L. Herter, J. Appl. Phys. **72**, 273 (1992).
[10] A. G. U. Perera, W. Z. Shen, H. C. Liu, M. Buchanan, M. O. Tanner, and K. L. Wang, Appl. Phys. Lett. **72**, 2307 (1998).
[11] F. Merlet, B. Pajot, Ph. Arcas, and A. M. Jean-Louis, Phys. Rev. B **12**, 3297 (1975).
[12] P. J. Dean, Y. Yafet, and J. R. Haynes, Phys. Rev. **184**, 837 (1969).
[13] D. G. Esaev, M. B. M. Rinzan, S. G. Matsik, A. G. U. Perera, H. C. Liu, B. N. Zhonkov, V. I. Gavrilenko, and A. A. Belyanin, J. Appl. Phys. **95**, 512 (2004).
[14] F. Raissia and N. A. Sheenib, Sens. Actuators, A **104**, 117 (2003).
[15] Aaron R. Hawkins, Thomas E. Reynolds, Derek R. England, Dubravko I. Babic, Mark J. Mondry, Klaus Streubel, and John E. Bowers, Appl. Phys. Lett. **68**, 3692 (1996).
[16] M. D. Petroff, M. G. Stapelbroek, and W. A. Kleinhans, Appl. Phys. Lett. **51**, 406 (1987).
[17] D. G. Esaev, S. G. Matsik, M. B. M. Rinzan, A. G. U. Perera, H. C. Liu, and M. Buchanan, J. Appl. Phys. **93**, 1879 (2003).
[18] R. F. Kirkman, R. A. Stradling, and P. J. Lin-Chung, J. Phys. C **11**, 419 (1978).
[19] A. Onton, P. Fisher, and A. K. Ramdas, Phys. Rev. **163**, 686703 (1967).